ISSN: 2754-6675

Journal of Chemistry & its Applications

SCIENTIFIC Research and Community

Research Article

Open Access

Assembly and Electrostatic Steering of α-lactalbumin/ Lysozyme Heterodimers: Kirkwood Correlation

Yathrib Ajaj[1]* and Arbab I Arbab[2]

[1]Mathematics and Sciences Department, College of Science German University of Technology in Oman, Oman

[2]Department of Physics, College of Science Qassim University, KSA

SUMMARY

The interaction of LYS with native α-LA (holo α-LA) and its calcium-depleted form (apo α- LA) is investigated using Dielectric Relaxation Spectroscopy (DRS) and Dynamic Light Scattering (DLS). Here, the interaction between LYS and α-LA change the diffusion coefficient of substrate and newly formed oligomer exhibit its characteristic Brownian motion, as followed by DLS. We report on our efforts towards the understanding of the interaction occurring between these two proteins. To describe the possible, assemble in more detail, protein-protein docking simulations was provided. In a docking simulation, several putative structural models of heterodimers are selected by scoring functions from an ensemble of many heterodimer models. The low docking score of these models was used to obtain theoretical values of the dipole moment and hydrodynamic radius using PHEMTO Server and HYDROPRO program, respectively.

***Corresponding author**

Yathrib Ajaj, Mathematics and Sciences Department, College of Science German University of Technology in Oman.

Received: July 18, 2024; **Accepted:** July 23, 2024; **Published:** August 23, 2024

Keywords: Dielectric, Kirkwood, α-lactalbumin, Lysozyme, Dimer, Hydrodynamic, Dipole Moment, Debye, Tumbling Time, DLVO

Introduction

70%−80% of all proteins are thought to be permanently oligomeric; that is, they are composed of multiple proteins that are held together in precise spatial organization through a multiple intermolecular interactions of weak energy (hydrogen bonding, electrostatic interactions, Van der Waals interactions, etc.). Although it is of great fundamental interest to understand the physicochemical basis of protein self-assembly as shown for α-LA that arrange into fibrils, spherical particles or aggregates depending upon the physicochemical conditions of the medium. The mastery of protein- protein interactions (PPIs) would also allow access to novel biomaterials with nature's favorite and most versatile building block. Hence, understanding the driving forces that trigger protein self-assembly and the successive steps leading to the building of supramolecular structures is of paramount importance for controlling their shape, size and properties [1-7].

α-lactalbumin (α-LA) and lysozyme (LYS) share only 40% identity in amino acid sequences but they have a closer spatial structure and gene organization. Although structure similar, functionally they are distinct. LYS bind and cleave the glycosidic bond linkage in sugars, whereas, α-LA does not bind sugar but participates in the synthesis of lactose. α-LA binds several metal ions, including calcium, which is thought to play a role in the regeneration of native α-LA from the reduced denatured form, where as, only a few types of LYS bind calcium [8]. α-LA also has a distinct zinc binding site that is thought to play a role in the binding of the lactose synthase [9]. They differ also in their isoelectric points. α-LA is an acidic protein with pI ~ 5, while LYS is a basic protein and has pI around 10.

These two proteins uniquely co-exist in mammalian milk. It is intriguing that the unique co- existence of LYS and α-LA should have a myriad of functions. Since LYS is a basic protein while α- LA, by contrast is an acidic protein, the two proteins would associate via electrostatic interaction.

A number of experimental studies have focused on the heterogeneous assembly of LYS and various forms of α-LA [10-14]. Ibrahim et al. reported a distinct association of LYS with α-LA involving dimerization and that α-LA molecule appears to compete on binding the same dimerization site of LYS molecule. A complex of α-LA/LYS at one molar ratio exhibited antibacterial activity against Gram- positive *Staphylococcus aureus* and Gram-negative *E. coli* K-12 [12].

Nigen et al investigated the interaction between LYS and the two structural forms of α-LA using isothermal titration calorimetry [6]. From their results, it was apparent that LYS did not interact with a native calcium-loaded α-LA (holo α-LA) but did interact with calcium-depleted α-LA (apo α-LA) to form specific temperature-dependent supramolecular structures [6,13]. Protein self-assembly into supramolecular structures usually requires structural destabilisation or the formation of specific protein oligomers (nuclei) [15]. Based on their studies, α-LA destabilisation through the release of bound Ca2+ appears to be an important parameter

for the formation of structures at macroscopic level [6]. Recently, using fluorescence anisotropy, they confirmed that LYS and apo α-LA but also LYS and holo α-LA self-assemble as heterodimers [14]. However, conditions such as ionic strength and temperature have a large impact on protein self-assembly [6,14].

Experimentally, it is important to obtain an unambiguous measurement of protein–protein interactions under a variety of solution conditions. Traditionally, protein structure determination to atomic resolution has been aimed at a single static conformation that agrees with the experimental data. However, transient excursions from the ground state, i.e. protein dynamics, pertain to the mechanisms of protein functions, including macromolecular association [15]. Thus, characterization of protein dynamics presents a challenging yet exciting theme in biophysics and structural biology. Among the different approaches that have been explored to quantify protein–protein interactions, measurement of protein dynamics has been an elusive scientific goal for elucidating the full panoply of protein-protein interaction.

Material and Instrumentation

Reagents

Hen egg white lysozyme, LYS, (≥ 90%, L 7651) and bovine holo-α-lactalbumin, holo α-LA, type 1 (≥ 85%, L5385) were purchased from Sigma-Aldrich as dialyzed and lyophilized powder and used without further purification. Apo α-lactalbumin (apo α-LA) was prepared by dialysis of a solution of holo α-LA against deionized water at pH 2 for 48 h at 4 °C using a dialysis membrane (Slide-A-Lyzer Dialysis Cassettes, Pierce Company) with a nominal cutoff of 3.5 Da to remove calcium ions. The pH of the apo α-LA solution was adjusted again to pH 7 with 1 M NaOH and then freeze-dried.

Stock solutions of LYS, holo α-LA, and apo α-LA were prepared by solubilization of protein powders in 30 mM Tris-HCl, buffer (pH 7.0). They were filtered through a 0.2 μm membrane before preincubation at the working temperature. The protein concentrations were determined by measuring the absorbance at 280 nm using extinction coefficients of 28540 L mol-1 cm-1and 38782 L mol-1 cm-1for α-LA and LYS, respectively.

Dielectric Dispersion Relaxation

The experimental techniques mentioned before were used to monitor the real part ε ′(*v*) (dielectric dispersion) and imaginary part
ε ′(*v*) (dielectric loss) of the complex permittivity, ε *(*v*) In the frequency range 300 kHz $\leq \nu = \omega/2\pi \leq$ 1.3GHz we employed the network analyzer 8712 ES (Agilent Technology) with a coaxial line terminating in the sample cell of Kaatze's design16. At 200 MHz ≤ *v* ≤ 20 GHz, the network analyzer HP 8720 (Hewlett Packard) and the probe HP 85070B was utilized. The experimental uncertainty was within the range 1-10 % at all the frequencies. Spectra were recorded five times at 298.15 K.

The hydrodynamic of protein effects its association due to irregular protein surfaces shapes, therefore, proteins were assume as close to spherical as possible. When the total number of spherical molecules in the protein solution is N, and the dipole moment of the i-th particle is m_i, one can write for the macroscopic dipole moment M as:

$$\mathrm{M}(x) = \sum_i^N \tilde{m}_i(x) \qquad (1)$$

where x denotes the set of position and orientation variables of all molecules and tilde ˜ to indicate the microscopic or molecular significance. In the case of non-polarizable molecules the average of the square of the total moment can be calculated as follows:

$$\left\langle \mathrm{M}^2 \right\rangle = N g_k \left\langle \tilde{m}_j \sum_i^N \tilde{m}_i \right\rangle \qquad 2$$

The above equation is so called Kirkwood relation [15-23]. The Kirkwood factor, g_K, can have values greater and less than one and this accounts for the preferred dipole alignment (parallel or anti-parallel). Thus, a detailed evaluation of the g_K provides detailed account into the orientation of the dipoles thereby revealing information about protein self-assembly.

Dynamic Light Scattering

Within this section, DLS measurements were made on the fixed scattering angle Zetasizer Nano-S system (Malvern Instruments Ltd., Malvern, UK) with a He-Ne gas laser. Samples were measured in a low volume disposable sizing cuvette. The light scattering was detected at 173º and collected in automatic mode, typically requiring measurement duration of 90 seconds. The resulting data were analyzed using the "Zetasizer Nano software" Version 6.10 (Malvern Instruments Ltd., Malvern, UK). The viscosity of the sample and dispersant was measured using Automated Micro Viscometer (AMVn, Anton Paar) at 25.0 ºC.

For the characterization of the interaction of two different proteins, an experimental method known as the Mole Ratio Methods was used. This technique holds the concentration of one of the two components constant, while varying the amount of the other components. A measurable parameter proportional to complex formation, such as ultraviolet-visible absorption or enzymatic activity, is plotted against the mole ratio of the two components. Here, we used the average hydrodynamic radii, r_{avg}, as the measurable parameter.

There are two common methods used to analysis autocorrelation functions, namely cumulants and regularization [24,25]. Cumulants analysis determines an intermediate hydrodynamic radius based on all species present in solution. Zetasizer software fit the DLS autocorrelation functions to a cumulants analysis "defined in ISO13321 Part 8", truncated at the second cumulant term. Cumulants analysis determines an average translational diffusion coefficient, *Dz* , where the subscript z indicates weighting by the relative intensity of light scattered by each species, as:

$$D_z = \sum_i D_{t,i} I_i \qquad (3)$$

where $D_{t,i}$ represents the translational diffusion coefficients for each species and I i the relative scattering intensities from each species [26]. For proteins with $r_h \leq 20$ nm, there is no significant angular dependence to the intensity of scattered light from the samples, and the intensity of light scattered from a single species is proportional to the molar mass and concentration, then:

$$D_z = \frac{\sum_i M_i^{\,2} \cdot c_i \cdot D_{t,i}}{\sum_i M_i^{\,2} \cdot c_i} \qquad 4$$

The hydrodynamic radius is calculated from the translational diffusion coefficient using the Stokes-Einstein relation:

$$r_h = \frac{k_B T}{3\pi\eta D_t} \quad (5)$$

To convert the diffusion coefficients to radii, we set:

$$r_{avg} = \frac{\sum_i M_i^{\,2} \cdot c_i}{\sum_i M_i^{\,2} \cdot c_i / r_i} \quad (6)$$

where ri represents the hydrodynamic radii of the species. r_{avg} is the cumulants " r_h " value reported by DLS analysis software. The "avg" subscript represents the average of several species. Then, the measured r_{avg} may be modeled using molar masses, molar concentrations, and radii of the constituent species. DLS measurements of each mixture over a range of A_{tot}: B_{tot} enough data to extract the reaction equilibrium constant.

Although a single measurement of r_{avg} obviously cannot characterize the mixture of species present in solution, multiple measurements over a series of concentrations can result in an accurate characterization. This is the underlying principle of the Mole Ratio Methods. Molar concentrations of monomer and complex in solution were modeled using standard chemical equilibrium relations and the known total concentrations of A and B . For example, for the postulated reaction: A + B ↔ AB the equilibrium dissociation constant is given as:

$$k_d = \frac{[A]\cdot[B]}{[AB]} \quad (7)$$

For known total molar concentrations of two proteins $[A_{lot}]$ and $[B_{lot}]$, the molar concentrations of free solution unassociated [A] and [B] and the complex [AB] may be calculated based on an assumed k_d. To calculate the molar concentrations [A], [B], and [AB]:

$$[A_{tot}] = [A] + [AB], \qquad [B_{tot}] = [B] + [AB] \quad (8)$$

then:

$$[A] = \frac{[A_{tot}]}{1 + \frac{[B]}{k_d}} \text{ and } [B] = -\frac{1}{2}([A_{tot}] - [B_{tot}] + k_d) - \left\{([A_{tot}] + [B_{tot}] + k_d)^2 + (4[B_{tot}]k_d)\right\}^{\frac{1}{2}}$$

Hydrodynamic Radius

To estimate the rotational correlation time of heterodimer that would take into account size and topology of the protein HYDROPRO program was employed. The harmonic mean rotational correlation time of α-LA/LYS heterodimer was calculated from the atomic-level structure (Dock PDB file) using the bead-modeling methodologies [27,28]. Briefly, the procedure starts from building a primary hydrodynamic model by replacing non-hydrogen atoms with spherical elements of fixed size. The resulting primary hydrodynamic particle, consisting of overlapping spheres, is used to construct a shell model. For the heterodimer the atomic element radius was taken as 2.6 Å. The shell of overlapping spheres is filled by smaller spheres, that are act as point sources of hydrodynamic friction. Then, the radius of the small spheres is extrapolated to zero. The model building and calculation were carried out with HYDROPRO public domain software, version 5a. In this calculation, we used a bulk solvent viscosity of η_0 = 0.892 cP as for H_2O at 298.15 K.

The theoretical hydrodynamic radius, r_h, can be also calculated based on correlations of the volume−molecular mass

where ϕ is the partial specific volume of the protein ($\phi = \frac{1}{\rho}$), h is the hydration for soluble proteins (0.35 g of H_2O) and η is the viscosity. Protein densities were calculated according to this formula:

$$\rho = \left[1.41 + 0.145 \cdot \exp - \left(\frac{M_{wt}}{13}\right)\right] \quad (11)$$

where ρ is the protein density in g cm^{-3}, M_{wt} is the molecular weight in kDa obtained from "Protein Calculator v3.3"

Dipole Moment

Protein pH-dependent Electric Moment Tools (PHEMTO) is a web server for evaluating protein electrostatic characteristics relative to their molecular interactions. Input is the atomic coordinate file in PDB format; output is electric/dipole moments and interactive visualization as well as the full electrostatic characteristics [29-56]. In particular, the donor and acceptor potentials and *pKa*'s of all participants in the hydrogen bonding network are evaluated by the server. The program allows variation of pH, as a result of which the potential-values and *pKa*-values are varied. The model for protein electrostatics can be built on the assumption for continuum medium description, fixed atom approximation, protein–solvent boundary numerically described by atomic static accessibilities, solvent accessibility (SA) and two types of charges, the permanent (pH-independent) partial charges and proton-binding sites with pH-dependent titrable charges. Since the ratio of the number of ionic amino acids (N_{ion}) and the total number of amio acids (N_{tot}) is relative high for protein particles with small radii (R_p), the pairwise interaction between any *i*-th and *j*-th ionic groups counts contributions from charge-charge, charge-dipole and dipole-dipole interactions, which can be simulated by an empirical three exponential curve:

$$W_{ij}(r, a_k) = \sum_k \left(\frac{a_k}{r_{ij}}\right) \quad (12)$$

where k = 1 for long-range (Columbic) interactions; k = 2 for mid-range, charge–dipole interactions; and k = 3 for short-range dipole–dipole interactions. The a_k were estimated by a non-linear procedure by minimizing the functional F (a_1 , a_2 , $a3$):

$$F(a_1, a_2, a_3) = \int \mathrm{pH}_i \left\{\left[\frac{\partial Z^{\exp}(\mathrm{pH}_i)}{\partial \mathrm{pH}}\right] - \left[\frac{\partial Z^{th}(\mathrm{pH}_i, a_1, a_2 a_3)}{\partial \mathrm{pH}}\right]\right\}^2 \quad (13)$$

where the values of Z^{exp} are taken from experimental data and Z^{th} are the calculated values of the protein net charge as a function of pH. The initial values of the coefficients a_k are obtained by numerical approximation of W (r_{ij}). Through extensive testing, using large dataset of structures, it was found that a1 , a2 and a3 values are practically constants for a great number of proteins. The pH- dependence of the electrostatic potential $\Phi_{el,i}$ (pH) at the *i*-th proton binding site in PHEI was evaluated according to the following equation:

$$\Phi_{el,i}(\mathrm{pH}) = 2.3RT\sum_{j\neq i}\left\{Q_j(\mathrm{pH})W_{ij}\left[1-\frac{SA_i+SA_j}{2}\right]\right\} \qquad 14$$

Here Q_j (pH) is defined by the degree of dissociation or statistical mechanical proton population of given H^+-binding site;

$Q_j(\mathrm{pH}) = (1-s_j)$ and $Q_j(\mathrm{pH}) = -(s_j)$ for basic and acidic groups, respectively. Using partial titration of each j-th group we can find the pH-dependent net-charge of the whole molecule, Z Z(pH), i.e. potentiometric titration curve:

$$Z(\mathrm{pH}) = \sum_j Q_j(\mathrm{pH}) \qquad 15$$

By definition if 0 = Z then pI pH = , i.e. the isoelectric point (the only pH at which the dipole moment of a protein molecule can be evaluated)

PHEMTO server attempts to explore protein charge distributions in terms of electric/dipole moments by treatment of pH-dependence and self-consistence. The server provides an algorithm to solve for molecular electrostatic potential (MEP) with explicit account for reaction field effects. Solve the nonlinear Poisson-Boltzmann equation with special attention given to reaction field contribution, Born salvation, term was applied:

$$\nabla\{\varepsilon(r)\nabla\Phi(r,\mathrm{pH})\} = -4\pi\rho(r,\mathrm{pH}) - \kappa^2\sinh(\Phi(r,\mathrm{pH})) \qquad 16$$

where ρ(r, pH), pH-dependent charge density, is obtained by pH-dependent self-consistent iterative procedure and used as input for numerical Poisson-Boltzmann solver to obtain pH-dependent electrostatic potential (EP) grid, Φ(r, pH); ∇ is the standard 'nabla' operator from vector calculus, κ is the reciprocal of Debye length, which accounts for ionic strength and measures how fast EP drops by

Results and Discussion

Dielectric dispersion spectroscopy

The complex dielectric permittivity of an electrically conducting system is given by

$$\varepsilon^*(\nu) = \varepsilon'(\nu) - i\varepsilon''(\nu) = \varepsilon_\infty + \Delta\varepsilon'(\nu) - i\Delta\varepsilon''(\nu) + \sigma/i\varepsilon_0 2\pi\nu \quad (i^2=-1) \qquad 17$$

As usual, the static (d.c.) conductivity σ gives rise to a low-frequency response of $\varepsilon''(\nu)$, which diverges as $\sigma/i\varepsilon_0 2\pi\nu$, where ε_0 is the permittivity of the vacuum. The conductivity of the buffer solution at pH 7.0 was $\sigma \approx 0.2\ \Omega^{-1}\ \mathrm{cm}^{-1}$, those of the protein solutions were up to three times as large.

Figure 3.1 shows the real part, $\varepsilon'(\nu)$, imaginary part, $\varepsilon''(\nu)$, and conductance-corrected imaginary part $\varepsilon''(\nu) - \sigma/2\pi\nu$ of 1.7 mM holo α-LA/LYS and apo α-LA/LYS mixtures. The key interest lies in the relaxation terms $\Delta\varepsilon'(\nu)$ and $\Delta\varepsilon''(\nu)$. Electronic and vibrational processes are often calculated for by a limiting value $\varepsilon_\infty = n^2$ of the real part, where n is the optical refractive index Owing to processes in the terahertz regime, dielectric relaxation data for pure water below 100 GHz extrapolate, however, to $\varepsilon_\infty = 5.5$. The latter value was adopted in further data processing. The results proved to be insensitive to moderate variations of ε_∞, by ± 1 say.

The relaxation curves (Figures 3.3) can be broken down into three principal regions, namely, β, δ, and γ. From β-relaxation (100 kHz-100 MHz) one gains insight into the molecular shape, size and the dipole moment of proteins. γ-dispersion corresponds to the reorientaional relaxation due to bulk water and observed around 10 GHz. Between β- and γ-dispersion there is small relaxations associated with intramolecular motions and protein-water coupling as discussed before (Chapter 3). It must be borne in mind that since this Chapter is dealing with protein assembly, the interest will mainly focuses on β-relaxation [57].

All spectra, namely, the complex permittivity ε^* vs frequency (ν), were fitted by a superposition of two Debye processes (2D):

$$\varepsilon^*(\nu) = \varepsilon_\infty + \sum_{j=1}^{2}\frac{\varepsilon-\varepsilon_j}{1+2i\pi\nu\tau_j} \qquad 18$$

By separation of the above equation into real, $\varepsilon'(\nu)$ and imaginary, $\varepsilon''(\nu)$ parts we get:

$$\varepsilon'(\nu) = \varepsilon_\infty + \sum_{j=1}^{2}\frac{S_j}{1+(2\pi\nu\tau_j)^2} \qquad 19$$

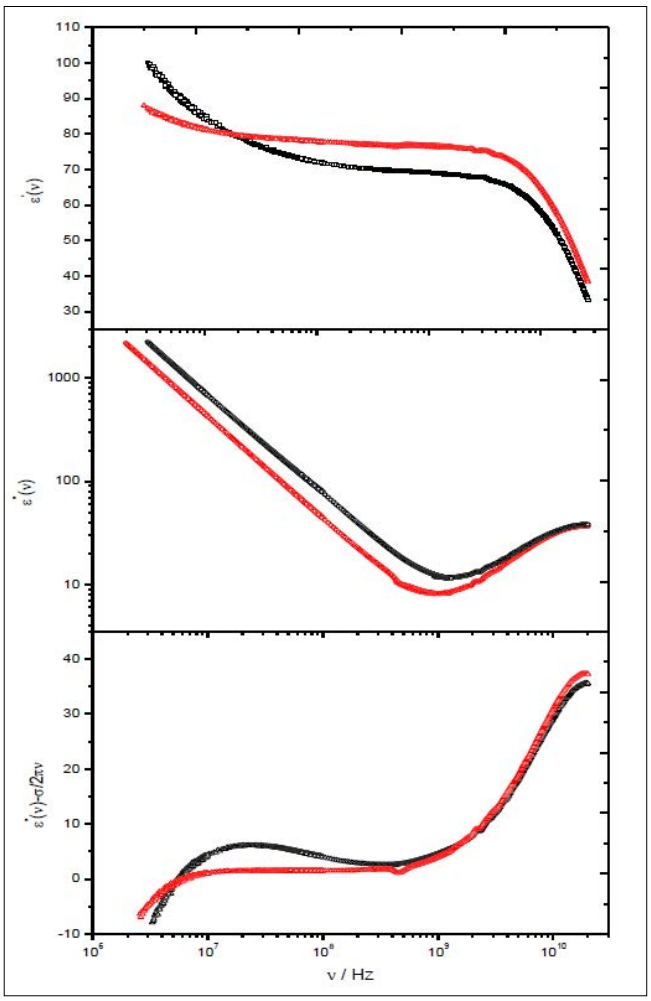

Figure 1: Real, imaginary and conductance-corrected imaginary part of the dielectric spectrum of holo α-LA/LYS (red) and apo α-LA/LYS (black) in 1.7 mM, 40 mM Tris-HCl buffer, pH = 7.0, and at 298.15 K.

$$\varepsilon''(\nu) = \varepsilon_\infty + \sum_{j=1}^{2} \frac{2\pi\nu \cdot S_j}{1 + (2\pi\nu\tau_j)^2} \qquad 20$$

In the above relations, $S_j = \varepsilon_j - \varepsilon_{j+1}$ (this is the amplitude of the relaxation), $\varepsilon_S = \varepsilon_\infty + \sum S_j$ where ε' is the static-permittivity (zero-frequency) of the protein, τ_j corresponds to the relaxation time. Parameterization of the spectra along with the standard deviation (SD) is summarized in Table 2 and 3. The values given are for two different conformational state, holo α-LA and apo α-LA. All spectra were recorded at pH 7.0 and 298.15 K.

Effect of intermolecular interactions on relaxation time and hydrodynamic radius

First, the variation of protein tumbling time, τ_β (ns), for holo α-LA/LYS and apo α-LA/LYS complex concentrations will be discussed. The change of tumbling times are shown in Table 1, Table 2 and Figure 2.

Table 1: Parameterization of the dielectric spectra for LYS/ holo α-LA solutions

C / mM	τ_β / ns	S_β	ε_S
0.50	46.21	9.71	89.35
1.05	48.61	13.18	93.47
1.70	49.14	13.47	93.48
2.40	52.91	15.93	96.27
3.00	63.20	20.40	101.46
4.00	67.27	26.15	106.80

Table 2: Parameterization of the dielectric spectra for LYS/ apo α-LA solutions

C / mM	τ_β / ns	S_β	ε_S
0.50	27.91	23.59	101.37
1.05	32.93	24.01	103.57
1.70	38.19	28.92	109.70
2.40	41.58	31.34	114.07
3.00	46.39	34.97	118.78
4.00	48.81	64.46	148.88

Some interesting effects can be observed from Figure 4. First, increasing protein concentration leads to the increase of the correlation time of Brownian protein tumbling. At these concentrations the mean distance between neighboring protein molecules in solution is comparable to the size of the proteins. Thus, intermolecular interactions may appreciably affect the tumbling time. It is obvious that the increase of the concentration is about 1.5-fold.

Second, the tumbling times for holo α-LA/LYS and apo α-LA/ LYS mixtures are different. This suggests differences in the conformation of the heterodimers in accordance with the way of interaction due to the Ca^{2+} releasing. It was reported, for instance, that, in the absence Ca^{2+} at natural pH, α-LA adopts molten globule state, and the interaction of apo α-LA with LYS could be promoted with overall conformational changes.

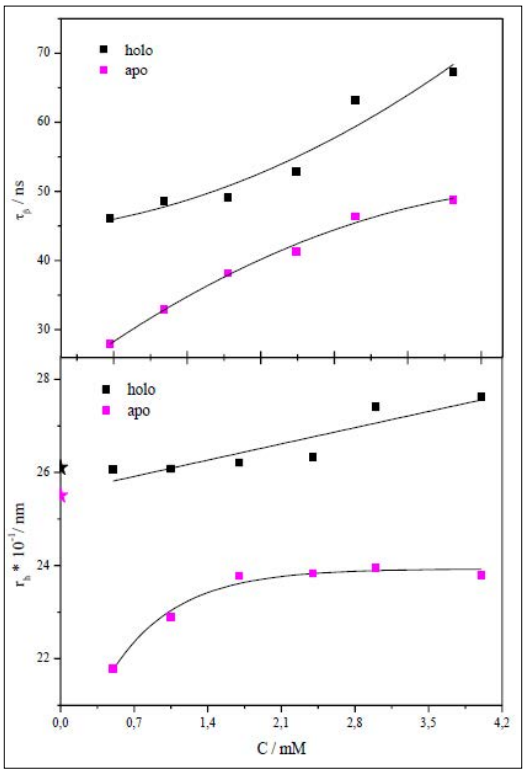

Figure 2: Reorientation time, τ_β, and Stokes radius for complexes, r_β for LYS interacting with holo α-LA (black) and apo α-LA(magenta) at various complex concentration. Lines are for visualization only.

Interestingly, the tumbling time for holo α-LA/LYS is higher than that expected for the heterodimer. From theoretical calculations, one should have obtained tumbling time in the range of 32- 35 ns, as also observed for the LYS homodimer (data not presented) which possess almost the same molecular mass as α-LA/LYS heterodimer. One plausible rational is the association-induced conformational change in both proteins, likely the partial unfolding. Another rational is the formation of higher oligomers. Using chemical cross-linking, Ibrahim et al have commented that in addition to the formation of heterodimer, α-LA and LYS also assemble to form higher order oligmers. The densitometric of the higher oligmers is around 8.3%. DRS needs an amount of 25% of the oligomers to increase the reorientation time.

On the other hand, apo α-LA/LYS exhibits a tumbling time that can be reasonably assigned to the relaxation of heterodimer. Nigen et. Al, conclude that assembly of apo α-LA and LYS into organized supramolecular spheres takes place from a small aggregate, the dimer of the subunit [6]. Accordingly, a relaxation that develops with its frequency about 10 MHz is attributed to the relaxation of the dimer motion within the sphere and there is no effect at disposal for the tumbling of the whole sphere. The dielectric motion at MHz/GHz frequencies involves simultaneous cooperative reorientation of the molecules with $\tau = 1/\nu$.

The hydrodynamic radii, r_h, of α-LA/LYS complexes calculated from the Stokes-Einstein- Debye relation (SED) and displayed in Figure 3.5 offer more quantitative support. In the calculations of r_h, we assumed that both complexes are spherical particles and exhibit constant values for partial volume and hydration shell. It is obvious from the Figure 1 that there is no dramatic change in the hydrodynamic radius with concentration. For compression,

the hydrodynamic radii computed from HYDROPRO program using PDB docking files are also shown.

In the case of holo α-LA/LYS, extrapolation to infinite dilution yields $r_h \approx 2.6$ h r nm in perfect agreement with the result obtained from HYDROPRO and DLS. Based on correlations for the volumemolecular mass relationship of globular proteins (Equation 12), the intrinsic radius of holo α-LA/LYS is $r_h \approx 2.2$ nm. Similar differences between intrinsic and hydrodynamic radii have been observed for other proteins, and have been conducted to quantify the role of the hydration properties.

r_h calculated from SED relation suggests quite unequivocally that apo α-LA/LYS solution contained a significant fraction of protein dimers (Figure 1). This is in accordance with previous experimental evidence. An interesting point is the remarkable disagreement of experimental data with values calculated by HYDROPRO. SED values give $r_h \approx 2.2$ nm upon extrapolation to zero concentration (or infinite dilution); on the other hand, the HYDROPRO program yields $r_h \approx 2.57$ nm. Apo α-LA interacts with LYS to form heterodimer, which associates further into "insoluble" precipitates (supramolecular microsphere). The association into microsphere includes intra- and intermolecular packing which can be rationalised in terms of volume changes, given the dissimilarity of the hydrodynamic radii.

Another useful molecular information which can be obtained from τ_β using Stokes-Debye equation is the hydrodynamic volume:

$$\tau_\beta = \frac{3V_h\eta}{k_BT} \qquad 21$$

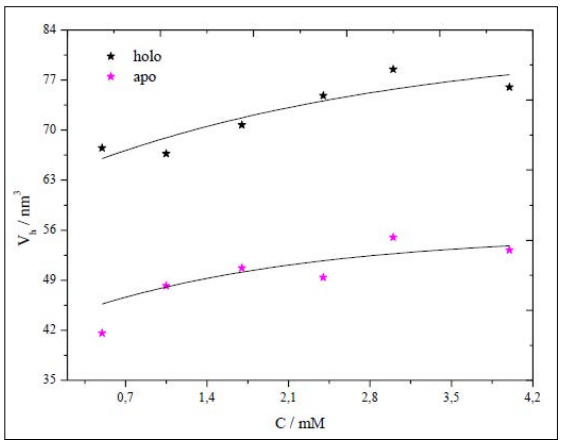

Figure 3: Hydrodynamic volume, V_h, for LYS interacting with holo α-LA (black) and apo α-LA (magenta) at various complex concentration. Lines are for visualization only.

Values of Vh calculated from Equation 3 using measured τ_β of α-LA/LYS mixtures are plotted in Figure 3 as a function of concentration. From the Figure, it was apparent that V_h is concentration- dependent.

A discrepancy between the hydrodynamic volume of holo α-LA/LYS and apo α-LA/LYS is due to conformational and structural differences and formation of insoluble aggregates.

Assignment of Relaxation Strength and Dipole Moment

The change of dielectric permittivity in the low-frequency segment of the dispersion curve can be ascribed to a change of the effective electric dipole moment, μ_{eff}, of the proteins upon assembly. The electric dipole moment enables one to understand electrostatic effects. From Tables 2 and 3, the static dielectric constant (the dielectric permittivity extrapolated to zero frequency, ε_S) increases with increasing concentration. This increase indicates a change in the chemistry of the protein solutions, such as protein assembly.

To study the dielectric relaxation strength of α-LA/LYS, plots of S_β against concentration of dispersed α-LA/LYS were displayed in Figure 4. Both mixtures show a noteworthy increase of the relaxation amplitude. From the amplitudes of relaxation processes, one can infer that the magnitude of the electrostatic strengths of holo α-LA/LYS and apo α-LA/LYS are rather completely different. This can be associated with the formation of supramolecular spheres [6]. The supramolecular spheres concentrate in insoluble liquid droplets that further coalesce and phase separate. As a result, one phase of the mixture is concentrated in the protein and the other phase contains mainly the solvent. Furthermore, with increasing protein concentration, the structures of the supramolecular spheres varied "increased", so that the relaxation strength was enlarged.

The presence of free charges and numerous discontinuities separating liquid phases in saturated emulsion give rise to Maxwell-Wagner polarization that may significantly affect the dielectric measurements [31]. Evidence suggests a complex interplay shaping the response of low-frequency (< 100 MHz) dielectric permittivity to changes if ionic charges present in interface between the two phases. Model calculations based on the Maxwell-Wagner-Hanai (MWH) theory can supported by direct measurements using DRS. The data can be predicted as a function of solution electrical conductivity (EC) as confirmed in limited tests. To analyze Maxwell-Wagner effect, the interface generally had to be charged by free charges and the electric field strength had to be infinite there. Since the Maxwell- Wagner effects give rise to a dielectric loss peak in the same frequency range as the protein dynamics appear, so, it is difficult to, accurately, differentiate the two processes.

The relaxation amplitudes are used to estimate the effective dipole moments, μ_{eff}, of the two mixtures. Recalling the most frequently employed Onsager-Oncley equation, allows one to calculate μ_{eff} of the solute:

$$\mu_{eff} = \sqrt{\frac{2\varepsilon_0 k_B T}{N_A c_p} S_\beta} \qquad 22$$

Variations of dipole moments of holo α-LA/LYS and apo α-LA/LYS with concentrations are shown in Figure 4. Extrapolating the curves to infinite dilution, molecular dipole moments of the two complexes are found to be ~ 550 D and ~ 850 D, respectively. Both solutions possess strong dipole moments since long-ranged, attractive interactions give a relative large contribution to μ_{eff}.

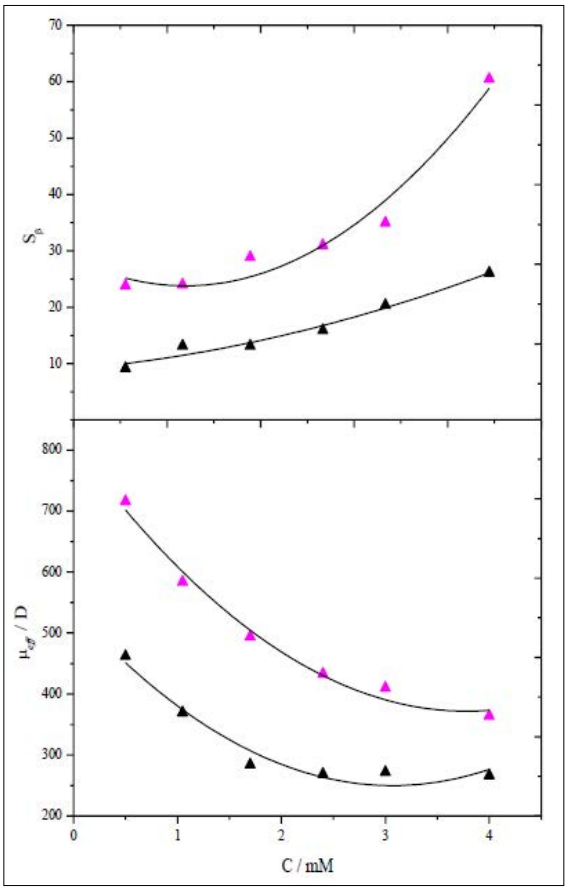

Figure 4: Amplitude, S_β , and effective dipole moment, μ_{eff} , for LYS interacting with holo α-LA (black) and apo α-LA (magenta) at various complex concentration. Lines are for visualization only.

It is obvious from Figure 4 that the effective dipole moment decreases with increasing protein concentration. Moreover, the concentration dependence of the effective dipole moments contains information about mutual correlations among the dipoles. The relation 27 was derived by the assumption that there is no inter-correlation among the dipoles of the protein [21]. Although, the variation of dipole moment here convincingly demonstrates that there is a strong correlation. In the subsequent section, based on the analysis of the Kirkwood factor, g_K , we underline the importance of such inter-correlation of dipoles in protein association processes.

Kirkwood correlation factor for α-LA/LYS heterodimers

The effective dipole moment is related to that of the isolated protein via:

$$\mu_{eff}^2 = g_K \mu_0^2 \qquad 23$$

where g_K is the Krikwood factor. The observed concentration-dependence of μ_{eff}^2 can only be founded in a decrease of the Kirkwood factor, g_K . As already noted, the general expression for the Kirkwood factor g_K is given by:

$$g_K = 1 + \sum_{j=1}^{N} \langle \cos\theta_{ij} \rangle \qquad 24$$

where θ_{ij} denotes the angle between the orientations of *i*-th and *j*-th dipole and the brackets denote the ensemble average. Here, we apply the same concept to deduce information about the assembly behaviour of α-LA with LYS.

The determination of g_K requires the dipole moment of the protein in the absence of dipolar correlations. In real systems, μ_0 depends on the net charge of the protein, which is dictated by the pH of the solution. Preliminary calculations indeed indicated a pH-dependent dipole moment of heterodimers. The reasonable and accurate way to evaluate the Kirkwood factor is to determined μ_0, which can be done theoretically using a defined pH, or by extrapolation of the effective dipole moment to zero protein concentration. The uncertainty of the data at low concentrations may allow a steeper extrapolation, so that this value is a lower limit.

Theoretical values give $\mu_0 \approx 720$ D for holo α-LA/LYS and $\mu_0 \approx 1050$ D for apo α-LA/LYS, which are higher than that obtained by extrapolation to zero-concentration (550 and 850 D, respectively). As noted by Antosiewicz, the experimental values of proteins dipole moment may of little value, because the conditions controlling the net charge of the protein are not specified [52].

Table 3: Kirkwood factors of holo α-LA/LYS and apo α-LA/LYS

C / mM	g_K (holo)	g_K (apo)
0.50	0.64	0.68
1.05	0.51	0.56
1.70	0.39	0.47
2.40	0.37	0.41
3.00	0.38	0.39
4.00	0.37	0.35

Table 4 shows that g_K decreased with increasing protein concentration. Such a behavior can be attributed to changes that result from strong antiparallel dipolar correlations between protein molecules, which are obviously favoured by their high dipole moments. It is known that α-LA interacts with LYS to form distinct aggregates such as heterodimer and/or multimers. The electrostatic attraction may be a responsible factor for the formation of aggregates.

The two major contributions to the interactions between colloids in aqueous solutions are Coulombic electrostatic interactions and van der Waals interactions. The sum of these forces describes the net force acting on colloidal particles and forms the basis of the well-known Derjaguin- Landau- Verwey-Overbeek (DLVO) theory of colloidal stability [58]. Due to the structural, functional, and surface anisotropy of protein molecules, their interactions are often dominated by contributions from relatively few, high-energy intermolecular configurations rather than by the overall colloidal interactions described by the DLVO theory. DLVO theory also often fails to describe interactions between

proteins at small distances due to either the breakdown of the continuum theory or emergence of non- DLVO forces [59]. Then, the long-range electrostatics interaction is the driving force of proteins assembly.

The present findings have some implication in the association kinetics of α-LA with LYS. For instance, the insoluble aggregate of apo α-LA/LYS is basically formed by the association of

heterodimer units. If the mixture has to form insoluble aggregate from the association of heterodimer, then it has to overcome the strong parallel orientations of the dipoles. These results emphasize the role of non-DLVO electrostatic interactions in assembly mechanism.

Thus, the Kirkwood factor reflects mutual compensation of dipole moments due to electrostatic interactions. This pronounced sensitivity to dipolar orientational correlations opens interesting possibilities for studying electrostatic protein-protein interactions. Thus, before α-LA and LYS associate to form a complex, they have to find the proper relative orientation by rotational diffusion. Orientational constraints limit the rate of association due to dipolar interactions between proteins and therefore lead to notable electrostatic steering of protein-protein associations, in addition to the effect of the direct Coulombic interactions between charged groups.

Influence of pH on holo α-LA/LYS assembly

The solution pH plays a crucial role for the protein interactions as it determines the charge distribution of the participating macromolecules. To illustrate this, DRS measurements were done at various pH (pH 4.5, 5.8 and 7.5) and condense the results into hydrodynamic radius and dipole moment.

The real part, ε′ (*ν*) of the spectrum is shown in Figures 1. The fit parameters are summarized in the Table 8 together with the hydrodynamic radii, r_h , and dipole moments, μ_{eff} . The attraction between α- LA and LYS is largest around neutral pH where both proteins have large, opposite net-charges. As pH is either decreased or increased the proteins go towards their fully protonated or de-protonated states and hence start to repel each other. If the pH is lowered, the surface charge is reduced. Thus, the so- called hydration forces which are a non-DLVO interaction prevent the protein particles from assembly.

At pH 4.5, α-LA and LYS coexisted in the mixed solution and apparently did not interact due to the repulsive Coulombic forces between the two positively charged proteins. The calculated hydrodynamic radius, r_h , was about ~ 2.03 nm, which correspondes to rh of the monomer proteins.

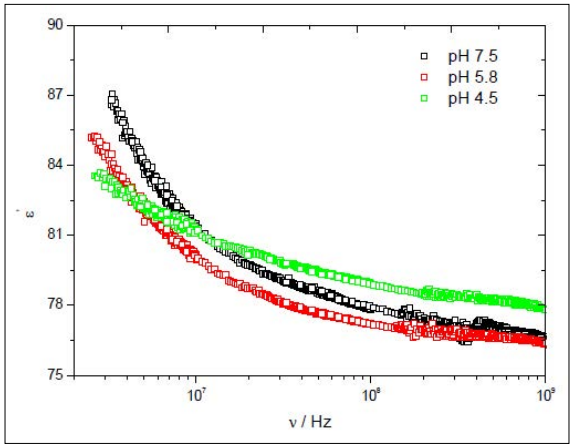

Figure 5: Real part of the dielectric spectrum of 1.7 mM holo α-LA/LYS. The curves refer to different pH.

On the other hand, μ_{eff} increases with decreasing pH. This effect is particularly large since long-ranged, attractive interactions give a relative large contribution to μ_{eff} .

Table 4: Parameterization of the dielectric spectra of 1.7 mM holo α-LA/LYS solution at three different pHs

pH	τ_β / ns	S_β	ε_S	r_h / nm	μ_{eff} / D
4.5	24.73	13.71	84.48	2.09	296
5.8	46.72	10.81	88.59	2.58	263
7.5	49.14	10.47	93.48	2.62	259

Dynamic Light Scattering

Table 5 shows the DLS results for different α-LA/LYS molar ratios, ranging from 0.05 to 1.5. Association was observed for all the protein molar ratios that were studied. The data show that the average size of the resultant particles is progressively increased with an increase in the added amount of α-LA to LYS, suggesting protein assembly. Moreover, as shown by the increase in the distribution width, the polydispersity of the aggregates increased with an increasing molar ratio.

The average size, ravg , of the aggregates depended on holo α-LA/LYS molar ratio, however, to lesser extent than that of apo α-LA/LYS aggregates observed for the same molar ratio range. The average size of the holo α-LA/LYS estimated to range from 2.5 to2.8 nm. On the other hand, the average size increases approximately to 1000 nm upon addition of various molar ratios of apo α-LA.

Table 5: Size distribution parameters of heterodimer resulting from the interaction of α-LA with LYS at 25 °C in 30 mM Tris-HCl, and for different α-LA/LYS molar ratios

α-LA/ LYS molar ratio	Holo		Apo	
	z-average/ nm	distribution width/ nm	z-average/ nm	distribution width/nm
0.00	1.60	1.56	1.62	1.54
0. 05	1.85	1.89	245	426
0.10	2.32	2.06	620	265
0.25	2.45	2.36	488	447
0.50	2.82	3.36	768	478
1.00	2.87	2.73	980	446
1.50	2.88	3.65	1200	730

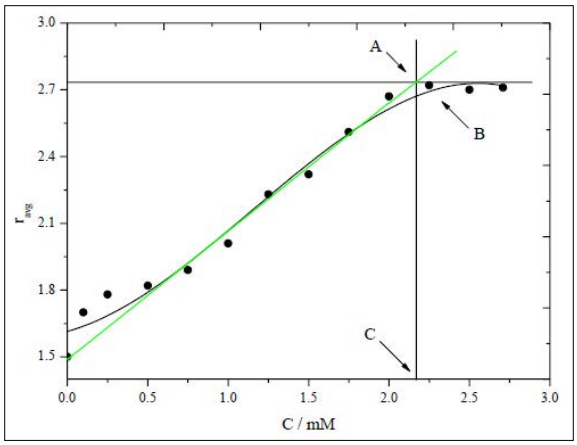

Figure 6: Hydrodynamic radius distribution derived from DLS data. The plot is a histogram of the scattering volume (fraction of total scatter volume) as a function of hydrodynamic radius.

At natural pH, α-LA was found to dimerize with LYS (Figure 6.). The self-assembly was measured at fix amount of LYS, 1.5 mM, and the data were fit simultaneously, with the monomer rh set to the measured value of 1.92 nm. The actual value for the mole ratio was calculated from the concentrations and volumes of the two proteins at the intersecting point (A). The hydrodynamic radius, rh , represented by the distance between C and B is rh of the heterodimer present in the equilibrium mixture. The fit yielded a parameter of 2.78 (± 0.3), corresponding to a heterodimer and in perfect agreement with the above results utilizing alternate techniques. The rh represented by the distance between A and B is rh of free (monomers) present in the equilibrium mixture. When fitting this system, we were able to fix the monomer rh to the value measured under nonassociating conditions, i.e., to the rh value at acidic pH. Doing so reduced the number of free parameters, and thus reduced the uncertainty of the results. Essentially identical results were achieved when the monomer rh was left as a free parameter. kd value at 25 °C was found to be ~ 35 μM, and inconsistent with data obtained by Nigen et al. The final DLS values obtained in this study are consistent with the formation of a holo α-LA/LYS heterodimer [60-66].

Conclusion

As mentioned previously, the combination of LYS with either holo α-LA or apo α-LA resulted in heterodimerity due mainly to electrostatic attraction as judged by DRS and DLS measurements. Here, the occurrence of specific electrostatic attraction has been reported following the interaction and assembly of α-LA with LYS, under specific physicochemical conditions. DRS observations showed that, at pH 7.0, the α-LA/LYS assembly leads to the formation of heterodimer. This study provides the dynamic behavior of aggregates. Higher oligomers, e.g. supramolecular structure, have relaxation time behind our frequency range. The hypothesis of protein association into dimers was further supported by DLS measurements. Simultaneously, these measurements excluded the possibility of forming linear aggregates of higher rank. Therefore, it was concluded that the combination of DRS and DLS can be

exploited as a convenient tool for determining and detecting not only the onset of protein aggregation in suspensions but also the form and composition of these aggregates.

Nigen et al reported that the calcium-depleted form of bovine α-LA (apo α-LA) interacts with LYS to form supramolecular structures with a diameter of ~ 1–6 μm, the DLS data confirmed these results. Why apo α-LA leads to completely different type of aggregates upon its assembling with LYS? A difference in protein surface charge density associated with Ca^{2+} removal may be a relevant reason. In fact, three negatively charged residues, Asp82, Asp87, and Asp88, are directly involved in calcium coordination and the removal of calcium leads to a more negatively charged α-LA, and that might probably promote the interaction with positively charged LYS. In addition, it was demonstrated that in the absence of calcium ion, α-LA adopts a molten globule-like state. Also, the removal of Ca^{+2} ions from α-LA shifts the midpoint of melting from 65 to 27 °C. As the half width of the melting interval of apo α-LA is ~ 20 °C, it follows that at 25 °C this form is just in the interval of its temperature transition. As a result, the behaviour of apo α-LA at 25 °C depends on subtle changes in the environment, which are difficult to control. Consequently, the interaction of apo α-LA with LYS could be promoted throughout the overall conformational changes.

DRS and DLS data show that the interaction between α-LA and LYS can be modulated by varying two parameters, ionic strength and pH. Electrostatic interaction is the driving force for α-LA and LYS assembly. Indeed, the formation of aggregates is governed by the ionic strength of the solution, increasing the ionic strength reduced the ability of α-LA and LYS to undergo assembling. The effect of ionic strength on α-LA/LYS assembly can be explained by shielding the surface charges of α-LA/LYS heterodimer which was also observed by Biesheuvel et al.

The long-range electrostatic interactions provide attractive forces between α-LA and LYS. However, the charge distribution on the two proteins surfaces is heterogeneous with the presence of charges and hydrophobic patches. Therefore, short-range interactions such as hydrogen bonding, hydrophobic associations or van der Waals attractions can be establish between the two proteins after the formation of heterodimer and stabilize the aggregates structures. This hypothesis is partly verified in the study of the solubility of apo α-LA/LYS macros by increasing the ionic strength of the solution. Indeed, in the case of apo α-LA/LYS and to destabilize the macroscopic aggregates, the ionic strength must reach concentrations well above those needed to inhibit the assembly. These results are in agreement with those of Selzer et al, who established that the increasing of the ionic strength lowered the association rate (k_{on}) due to the decrease in long-range electrostatic attraction. While the dissociation rate (k_{off}) is less affected by the ionic strength, due to structural reorganizations within the complex and the establishment of other types of short range interactions (e.g. hydrogen bonds, hydrophobic interactions and Van der Waals).

The results also show the existence of a link between the total proteins concentration and the fraction of proteins involved in the formation of oligomers. However, increasing the total protein concentration does not include all monomers into the aggregates, even at low ionic strength, i.e. a fraction of apo α-LA and LYS is always quantified in the soluble phase. The persistence of residual proteins in the soluble phase is frequently encountered during polymers assembly. The electrostatic interactions during polymers assembly is accompanied by release in counterions initially associated with individual molecules. This causes an increase of ionic strength of the opposing assembly of other proteins. This phenomenon is more pronounced than the initial ionic strength of the solution is low.

The formation and dynamic evolution of the protein assembly formed between two oppositely charged proteins show both interesting and intriguing. Therefore, further studies including structure techniques, e.g. NMR or X-rays, may be an appropriate approach to elucidate the formation of higher oligomers. It would be also interesting to characterize protein- protein assembly and determine its properties e.g. rheological and viscoelastic.

References

1. Ipsen R, Otte J, Qvist KB (2001) Molecular self-assembly of partially hydrolysed alpha-lactalbumin resulting in strong gels with a novel microstructure. J Dairy Res 68: 277.
2. Zhang S (2003) Fabrication of novel biomaterials through molecular self-assembly. Nat. Biotechol 21: 1171-1178.
3. Viney C (2004) Self-assembly as a route to fibrous materials: Concepts, opportunities and challenges. Curr Opin Solid State Mat Sci 8: 95.
4. Sanguansri P, Augustin MA (2006) Nanoscale materials development – a food industry perspective. Trends Food

Sci Technol 17: 547.
5. Goers J, Permyakov SE, Permyakov EA, Uversky VN, Fink AL (2002) Conformational prerequisites for alpha-lactalbumin fibrillation. Biochemistry 41: 12546-12551.
6. Nigen M, Croguennec T, Renard D, Bouhallab S (2007) Temperature affects the supramolecular structures resulting from alpha-lactalbumin-lysozyme interaction. Biochemistry 46: 1248-1255.
7. Takase K (1998) Reactions of denatured proteins with other cellular components to form insoluble aggregates and protection by lactoferrin. FEBS Lett 441: 271-274.
8. Permyakov EA, Berliner LJ (2000) α-Lactalbumin: structure and function. FEBS Lett 473: 269.
9. Ren J, Stuart DI, Acharya KR (1993) Alpha-lactalbumin possesses a distinct zinc binding site. Biol Chem 268: 19292-19298.
10. Howell NK, Yeboah NA, Lewis DFV (1995) Studies on the electrostatic interactions of lysozyme with α-lactalbumin and β-lactoglobulin. Int J Food Sci Technol 30: 813-824.
11. Howell N, Li-Chan E (1996) Elucidation of interactions of lysozyme with whey proteins by Raman spectroscopy. Int J Food Sci Technol 31: 439-451.
12. Ibrahim HR, Taniyama N, Aoki T (2004) Distinct Dimerization Between α-Lactalbumin and Lysozyme Exhibiting Novel Antimicrobial Activity against Gram-positive and Gram-negative Bacteria. Lett Drug Des Discovery 1: 101-109.
13. Nigen M, Croguennec T, Madec MN, Bouhallab S (2007) Dynamic and supramolecular organisation of α-lactalbumin/ lysozyme microspheres: A microscopic study. FEBS 274: 6085-6093.
14. Nigen M, Tilly V, Croguennec T, Drouinkucma D, Bouhallab S (2009) Molecular interaction between apo or holo α-lactalbumin and lysozyme: Formation of heterodimers as assessed by fluorescence measurementsBiochimica et Biophysica Acta 1794: 709.
15. Chiti F, Dobson C M (2006) Protein misfolding, functional amyloid, and human disease. Annu Rev Biochem 75: 333.
16. Göttmann O, Kaatze U, Petong P (1996) Coaxial to circular waveguide transition as high-precision easy-to-handle measuring cell for the broad band dielectric spectrometry of liquids. Meas. Sci. Technol 7: 525.
17. Grant EH, RJ Sheppard (1992) The dielectric properties of biological tissues: I. Literature survey. South, P. G., In: Dielectric Behaviour of Biological DOI 10.1088/0031-9155/41/11/001.
18. Takashima S (1989) Electrical Properties of Biopolymers and Membranes; Adam Hilger: Bristol. Ann Rev Phys Chem 43: 177.
19. Böttcher CJF, Bordevijk P (1973) Theory of Dielectric Polarisation; Elsevier: Amsterdam 2 https://shop.elsevier.com/books/theory-of-electric-polarization/luisa/978-0-444-41019-1.
20. Kaatze U (1993) Dielectric relaxation of H2O/D2O mixtures. J Chem Eng Data 203: 1-4.
21. Takashima S (2001) The structure and dipole moment of globular proteins in solution and crystalline states: Use of NMR and X-ray databases for the numerical calculation of dipole moment. Biopolymers 58: 398-409.
22. Höchtl P, Boresch S, Steinhauser O (2000) Dielectric properties of glucose and maltose solutions. J Chem Phys 112: 9810-9821.
23. Madden P, Kivelson D (1984) A Consistent Molecular Treatment of Dielectric Phenomena. Adv Chem Phys https://www.semanticscholar.org/paper/A-Consistent-Molecular-Treatment-of-Dielectric-Madden-Kivelson/0b1f27f364a09c3435431ef7b7bffc82de5be6f1.
24. Sacife BKP (1998) Principle of Dielectrics; Clarendon Press, Oxford.
25. Koppel DEJ (1972) Analysis of Macromolecular Polydispersity in Intensity Correlation Spectroscopy: The Method of Cumulants. Chem. Phys 57: 4814-4820.
26. Provencher SW (1979) Inverse problems in polymer characterization: Direct analysis of polydispersity with photon correlation spectroscopy†. Makromol Chem 180: 201.
27. Brown JC, Pusey PN, Dietz RJ (1975) Physical gels from PVC: dynamic properties of dilute solutions. Chem. Phys 62: 1136.
28. Hiemenz CP (1984) Light Scattering by Polymer Solutions in Polymer Chemistry: The Basic Concepts, Pub: Marcel Decker Inc, New York 659.
29. Garcia de la Torre J, Huertas ML, Carrasco B (2000) Calculation of hydrodynamic properties of globular proteins from their atomic-level structure. Biophys J 78: 719-730.
30. Halle B, Davidovic M (2003) Biomolecular hydration: From water dynamics to hydrodynamics. Proc Nat Acad Sci 100: 12135-12140.
31. Chalikian TV, Breslauer KJ (1996) Biopolymers 39: 619.
32. Forli S, Botta M (2007) Lennard-Jones potential and dummy atom settings to overcome the AUTODOCK limitation in treating flexible ring systems. Chem Inf Model 47: 1481-1492.
33. Chen R, Li L, Weng Z (2003) ZDOCK: an initial-stage protein-docking algorithm. Proteins 51: 80-87.
34. http://zdock.bu.edu/.
35. Ritchie DW, Kemp G (2000) Protein docking using spherical polar Fourier correlations. J Proteins 39: 178-194.
36. Schneidman-Duhovny D, Inbar Y, Nussinov R, Wolfson HJ (2005) PatchDock and SymmDock: servers for rigid and symmetric docking. Nucleic Acids Res 1: 363-367.
37. Schneidman-Duhovny D, Inbar Y, Nussinov R, Wolfson HJ (2005) Geometry-based flexible and symmetric protein docking 60: 224-231.
38. http://3.http//bioinfo3d.cs.tau.ac.il/SymmDock/.
39. http://bioinfo3d.cs.tau.ac.il/PatchDock/.
40. Comeau SR, Gatchell DW, Vajda S, Camacho CJ (2004) ClusPro: an automated docking and discrimination method for the prediction of protein complexes. Bioinformatics 20: 45-50.
41. Comeau SR, Gatchell DW, Vajda S, Camacho CJ (2004) ClusPro: a fully automated algorithm for protein-protein docking. Nucleic Acids Res 32: 96-99.
42. Comeau SR, Camacho CJJ (2005) Predicting oligomeric assemblies: N-mers a primer. Struct. Biol 150: 233-244.
43. http://nrc.bu.edu/cluster/cluspro_v1.cgi.
44. Tovchigrechko A, Vakser IA (2005) GRAMM-X public web server for protein-protein docking. Proteins 60: 296.
45. Tovchigrechko A, Vakser IA (2006) GRAMM-X public web server for protein-protein docking. Nucleic Acids Res 34: 310-314.
46. Lyskov S, Gray JJ (2008) The Rosetta Dock server for local protein-protein docking. Nucleic Acids Res 36: 233-238.
47. Gray JJ, Moughon SE, Kortemme T, Schueler-Fuman O, Misura KM (2003) D Proteins 52: 118.
48. http://www.ebi.ac.uk/msd-srv/capri.
49. Kremer F, Schönhals A (2002) Broadband Dielectric Spectroscopy, Springer-Verlag https://link.springer.com/book/10.1007/978-3-642-56120-7.
50. Böttcher CJF, Bordevijk P (1978) Theory of Dielectric Polarisation. Elsevier: Amsterdam 84: 1190-1191.

51. Antosiewicz J, Biophys J (1995) Computation of the dipole moments of proteins. Biophys J 69: 1344-1354.
52. Fischer H, Polikarpov I, Craievich AF (2004) Average protein density is a molecular-weight- dependent function. Protein Sci 13: 2825-2828.
53. Kantardjiev AA, Atanasov BP (2009) PHEMTO: protein pH-dependent electric moment tools. Nucleic Acids Research 37: W422-427.
54. Israelachvili J (1992) Intermolecular and surface forces, Academic Press, San Diego, CA, 2nd ed.
55. Mc Donald IK, Thornton JM (1994) Satisfying hydrogen bonding potential in proteins. Journal of Molecular Biology 238: 777-793.
56. Biesheuvel PM, Lindhoud S, Cohen Stuart MA, de Vries R (2006) Complex fluids with mobile charge-regulating macro-ionsPhys Rev E. DOI 10.1209/0295-5075/120/26001.
57. Biesheuvel PM, Lindhoud S, de Vries R, Cohen Stuart, Langmuir MA (2006) Phase Behavior of Mixtures of Oppositely Charged Nanoparticles: Heterogeneous Poisson−Boltzmann Cell Model Applied to Lysozyme and Succinylated Lysozyme 22: 1291-1300.
58. Chakrabarti P, Janin J Proteins (2002) Dissecting protein-protein recognition sites. Proteins 47: 334-343.
59. Reynolds Damerell, Jones (2008) Protorp: a protein-protein interaction analysis tool Bioinformatics https://www.researchgate.net/publication/23465959.
60. Sheffler W, Baker D (2008) RosettaHoles: Rapid assessment of protein core packing for structure prediction, refinement, design, and validation. Protein Sci 18: 229-239.
61. Selzer T, Albeck S, Schreiber G (2000) Rational design of faster associating and tigher binding complexes. Nature Structural Biology 7: 537-541.
62. Burgess DJ (1990) Practical analysis of complex coacervate systems. Journal of Colloid and Interface Science 140: 227-238.
63. de Vries R, Cohen Stuart M (2006) Current Opinion in Colloid and Interface Science. https://www.sciencedirect.com/journal/current-opinion-in-colloid-and-interface-science.
64. Weinbreck F, de Vries R, Schrooyen P, de Kruif, CG (2003) Complex coacervation of whey proteins and gum Arabic. Biomacromolecules 4: 293-303.
65. Turgeon SL, Schmitt C, Sanchez C (2007) Current Opinion in Colloid and Interface Science https://www.sciencedirect.com/journal/current-opinion-in-colloid-and-interface-science.
66. Henzler-Wildman K, Kern D (2007) Dynamic personalities of proteins Nature 450: 964-972.